ISSN 0029-3865

CBPF-CENTRO BRASILEIRO DE PESQUISAS FÍSICAS

Notas de Física

CBPF-NF-022/94
April 1994

Density Functional Study of Fe Bound to Ammonia

Joice Terra and Diana Guenzburger

Centro Brasileiro de Pesquisas Físicas, Rua Dr. Xavier Sigaud, 150, 22290-180, Rio de Janeiro/RJ, Brasil.

Abstract

Density functional calculations were performed to investigate the species formed by the interaction of an Fe atom and ammonia. The Discrete Variational method was employed and total energy calculations were performed for several configurations. It was found that the ground state is a ^{5}E, with Fe configuration $\sim 3d^{6.6}4s^{1.1}$; the Fe-N interatomic distance was determined to be 1.98$\mathring{A}$. The hyperfine parameters isomer shift, quadrupole splitting and magnetic hyperfine field were also calculated, and compared to reported experimental values obtained by Mössbauer spectroscopy in frozen ammonia.

Key-words: Fe-ammonia; Quadrupole splitting; Isomer shift.

1 Introduction

Transition metals may absorb ammonia strongly on their surfaces, even at room temperature. The heterogeneous catalytic synthesis and decomposition of ammonia is a subject of great technological importance [1]. Thus the understanding of the bonding mechanism between transition metals and ammonia is desirable. On the other hand, the technique of isolation of atoms and small molecules in frozen gases allows the use of solid-state techniques such as Mössbauer spectroscopy to probe charge and spin distributions. Accordingly, an investigation of Fe isolated in solid ammonia has been reported; the reaction product $FeNH_3$ was identified, and Mössbauer hyperfine parameters were measured [2]. However, it became evident that quantum chemical calculations would be needed to better understand the origin of the values obtained.

In this work, we report Density Functional Theory (DFT) calculations [3] for the species $FeNH_3$. The method employed is the Discrete Variational (DVM) [4]. We determine the ground state by performing total energy calculations for several electronic configurations. The charge and spin distributions are analysed. Finally, the Mössbauer hyperfine parameters isomer shift (δ), quadrupole splitting (ΔEQ) and components of the magnetic hyperfine field (H_F) are calculated and compared to experiment.

This paper is organized as follows: in Section 2 we briefly describe the theoretical method; in Section 3 we discuss the electronic structure, in Section 4 we report results for the hyperfine parameters and in Section 5 we summarize our conclusions.

2 Theoretical Method

In this section we describe briefly the main features of the DVM method [4] and give details of the calculations. The set of Kohn-Sham equations is solved (in Hartrees) [3]:

$$[-1/2\nabla^2 + V_c(\vec{r}) + V_{xc}^{\sigma}(\vec{r})]\phi_{i\sigma}(\vec{r}) = \varepsilon_{i\sigma}(\vec{r}) \tag{1}$$

In eqs. (1), the Coulomb potential V_c includes electron-nucleus and electron-electron interactions, and V_{xc}^{σ} is the spin-dependent local exchange-correlation potential of spin σ, as derived by von Barth and Hedin [5]. The Coulomb and exchange-correlation potentials are functionals of the electron density ρ_σ

$$\rho_\sigma(\vec{r}) = \sum_i n_{i\sigma}|\phi_{i\sigma}(\vec{r})|^2 \tag{2}$$

where $n_{i\sigma}$ is the occupation of molecular orbital $\phi_{i\sigma}$, which is allowed to be different for each spin σ in these spin-polarized calculations.

The molecular orbitals are expanded on a basis of numerical atomic orbitals

$$\phi_{i\sigma}(\vec{r}) = \sum_\mu \chi_\mu(\vec{r})C_{i\sigma}^{\mu} \tag{3}$$

obtained with atomic self-consistent-field local density calculations.

In the Discrete Variational scheme, minimization of the error functionals associated with each orbital $\phi_{i\sigma}$ in a three-dimensional grid of points leads to the secular equations:

$$([H] - [E][S])[C] = 0 \tag{4}$$

which are solved self-consistently until a desired criterion is met. In eqs. (4), $[H]$ is the hamiltonian matrix, $[S]$ the overlap matrix and $[C]$ the matrix of the eigenvectors, all the matrix elements being summations over the three-dimensional grid of points. In the present calculations, convergence was carried out to $< 10^{-4}$ in the charge and spin densities.

In order to calculate the Coulomb potential by one-dimensional integrations, the molecular charge density is fitted to a multicenter multipolar expansion [6]:

$$\rho(\vec{r}) \cong \sum_j d_j \sum_{\nu}^{I\,\prime} \sum_m C_{\ell m}^{\nu\lambda} R_N(r_\nu) Y_\ell^m(\hat{r}_\nu) \tag{5}$$

The summation is over a set I of atoms equivalent by symmetry, R_N are piecewise parabolic radial functions centered at atoms ν and λ distinguishes different basis functions of a given ℓ (j=I,ℓ, λ ,N). This expansion may be carried out to any degree of accuracy in the fit with the "true" density; in the present calculations, partial waves up to $\ell = 2$ were employed for Fe and N, and $\ell = 1$ for H; the least squares error of the fit of ρ was ~ 0.04.

The total energy E is defined as the expectation value (sum over integration mesh) of the energy density $e(\vec{r}_1\{R_\nu\})$. In order to control numerical errors, the actual computation of E is made by point-by-point subtraction of a reference system of non-interacting (NI) atoms, as in the basis, located at the nuclear sites $\vec{R}_\nu$:

$$E = \langle e(\vec{r}, \{\vec{R}_\nu\}) - e^{NI}(\vec{r}, \{\vec{R}_\nu\})\rangle + E^{NI} \tag{6}$$

Here we employed the algorithms of Delley and Ellis [7] to calculate E.

The variational basis set included all inner orbitals, e.g., no "frozen core" approximation was made. The valence functions included 3d, 4s and 4p on Fe, 2s, 2p and 3d on N and 1s, 2s and 2p on H. The self-consistent process was initiated with basis functions from the neutral atoms; after convergence, the basis was improved by generating atomic functions for atoms with configurations similar to those of the molecule. These are obtained by a Mulliken-type population analysis, in which the overlap population is divided proportional to the coefficients of the atoms [8]. This basis optimization process is repeated several times, until the configuration of the atoms in the molecule is approximatly the same as in the basis.

The three-dimensional grid of points was divided in two regions: the volume inside spheres placed around each nucleus, where precise polinomial integrations are performed on a regular grid [9], and elsewhere in space, where the pseudo-random Diophantine point generator is employed [4]. The spheres had radius: 1.8 a.u. (Fe), 1.0 a.u. (N) and 0.5 a.u. (H). A total of 12,700 points were used inside the spheres, and 2,200 Diophantine points elsewhere.

3 Electronic Structure

We performed self-consistent calculations for seven configurations derived by distributing 8 electrons among the spin-up and spin-down highest-energy valence molecular orbitals, originating mainly from the valence orbitals of Fe. In C_{3v} symmetry, the $3d_\sigma(z^2)$, 4s and $4p_\sigma(z)$ orbitals of Fe transform as the a_1 representation, and the $3d_\delta$ (x^2-y^2,xy), $3d_\pi$ (xz,yz) and $4p_\pi$ (x,y) transform as the e representation. Here the symbols σ, π and δ are employed in analogy to the linear molecules. For all configurations, the spin polarization resulted in a splitting of the spin-up and spin-down levels of a few eVs; thus the spin-up levels, of lower energy, were kept fully occupied.

In Table I are given the configurations considered, charges, Mulliken-type populations and magnetic moments. These last (in Bohr magnetons) are defined as the difference between the spin-up and spin-down populations. In Fig. 1 are plotted the total energies for the same configurations (relative to an arbitrary origin) for different Fe-N distances. The ammonia N-H interatomic distance and H-N-H angle were kept constant and equal to the experimental values in the gas phase (1.00 $\AA$ and 107.2^0) [10]. Determination of the N-H distance for the free NH_3 molecule, employing the same method described here, showed excellent agreement with experiment [11].

It is seen from Fig. 1 that the configurations with the lowest energies are **2, 3** and **3'**. These configurations are constructed by doubly occupying the $9a_1$ orbital, predominantly Fe $3d(z^2)$, and placing one electron in $10a_1\uparrow$, predominantly $4s\uparrow$. The orbitals $4e\uparrow$ and $5e\uparrow$, almost purely 3d(xz,yz) or 3d(x^2-y^2,xy), are also doubly occupied. The subtle difference between these three configurations is in the occupied spin down orbitals of e symmetry. In configuration **2**, the singly occupied orbital $4e\downarrow$ is predominantly 3d(xy,x^2-y^2); however, a non-negligible admixture with 3d(xz,yz) (17.4%) is present. In configuration **3** the singly-occupied orbital $5e\downarrow$ is almost totally 3d(xy,x^2-y^2) (98%) and in configuration **3'** (for which only a small interval of Fe-N distances was explored due to difficult convergence), the same singly occupied orbital is ~100% 3d(xz,yz). In **3** and **3'** the lower-energy $4e\downarrow$ is unoccupied.

The rationale behind the energy ordering **2<3<3'** is the following: configuration **3** has a slightly lower energy than **3'** since occupation of the d_δ orbitals, localized on a plane perpendicular to the Fe-N axis, leads to a smaller repulsion with the N lone pair on the same axis, as compared to d_π. Configuration **2**, with lower energy still, presents a mixture in orbital $4e\downarrow$ of d_δ and d_π, thus lowering the energy still by diminishing the interelectronic repulsion inside the 3d orbital. This configuration may be viewed as the Density Functional counterpart of a Configuration Interation calculation, formed by a mixture of two configurations, one with d_δ and the other with d_π occupation. It will be seen further on that the mixture of d_π and d_δ in orbital $4e\downarrow$ will prove essential in the interpretation of the measured quadrupole splitting.

All other configurations have significantly higher energies at all distances; thus the ground state of $FeNH_3$ is determined to be a ^5E with configuration **2**. It is interesting to notice the similarity with the ^6E ground state of the ion $FeNH_3^+$, as obtained with a modified coupled-pair functional (MCPF) calculation [12]; in fact, our ground state configuration corresponds approximatly to that obtained for the positive ion, with the addition of an electron to the $9a_1\downarrow$ (σ) orbital.

As seen in Table I, the Fe atom has a small positive charge in all cases, which is largest for the lowest-energy ^{5}E states (+0.22). Thus delocalization of charge towards the N stabilizes these configurations. The actual magnetic moment on Fe in the quintuplet ground state is somewhat smaller than 4 since, as may be seen in the Table, a small part of the spin is delocalized towards the Nitrogen.

From the Fe populations, it may be observed that the configuration in all cases is near $3d^74s^1$, more precisely $3d^{6.63}4s^{1.12}4p^{0.04}$ for the ground state. This means that dissociation would lead to Fe $3d^74s^1$ (^{5}F) instead of the Fe ground state $3d^64s^2$ (^{5}D) [13]. This may be understood as the need to promote approximatly one 4s electron into the more compact 3d orbital, to minimize repulsion with the N lone pair. It is interesting to observe that even for the two configurations in which the $10a_1 \uparrow$ orbital (mostly Fe 4s) was not ccupied (**4** and **5**), the 4s population is near 1.0. In these cases, the $9a_1 \downarrow$ orbital (partly 4s) is occupied, resulting in negative (antiferromagnetic) 4s orbital magnetic moments on Fe. The 4p populations obtained are very small in all cases.

As seen in Fig. 1, the equilibrium distance for the ^{5}E ground state is 1.98$\mathring{A}$. For all configurations except **4** and **5**, the minimum lies at distances slightly smaller than 2.0$\mathring{A}$. In the case of **4** and **5**, the smaller equilibrium distances obtained are due to non-occupancy of the diffuse $10a_1 \uparrow$ orbital. Interatomic distances obtained with Density Functional calculations compare well with experiment, being usually more accurate than Hartree-Fock [14]; however, the local density approximation in the exchange and correlation potential results in equilibrium distances which are usually underestimated by an average 0.05$\mathring{A}$ [15].

In Table II are displayed the d_σ, d_π and d_δ populations. We may notice the d_π-d_δ mixture, present in configuration **2**, and practically absent in all others. Another interesting feature is that for the configurations **2**,**3** and **3'**, with 3 electrons in $9a_1$ and $10a_1$, only have d_σ populations of 1.6-1.7. This is the result of mixing with the 2s and 2p orbitals of N, and consequent charge transfer towards the latter.

In Table III is given the valence orbitals population analysis for the ^{5}E (configuration **2**) ground state. It may be observed that the orbitals of a_1 symmetry are responsible for the 3d-4s hybridization on Fe, as well as mixture with N 2s and 2p.

In Fig. 2 are plotted the one-electron energy levels of predominantly Fe 3d nature, for the ^{5}E ground state (configuration **2**), as a function of the Fe-N distance. The spin-up and spin-down e-symmetry orbitals of predominantly d(xy, x^2-y^2) character become more stable than their counterparts at short distances, due to increased repulsion along the z axis and resulting increased antibonding character of the d orbitals with z components. For the same reason, the diffuse 4s ($10a_1\uparrow$) orbital has the highest energy at short distances, but is destabilized rather steeply as the Fe-N distance is increased.

4 Mössbauer Hyperfine Parameters

The isomer shift δ is defined as [16]

$$\delta = 2/3e^2\pi ZS'(Z)\Delta\langle r^2\rangle[\rho_A(0) - \rho_S(0)] \equiv \alpha\Delta\rho(0) \qquad (7)$$

where $S'(Z)$ is a correction for relativistic effects, $\Delta\langle r^2\rangle$ the variation of the mean square radius of the nucleus between excited and ground states of the Mössbauer transition, and

the electronic term in brackets is the difference between the density at the nucleus in the absorber and source. The density $\rho(0)$ is calculated with the use of Eq. 2. In a non-relativistic calculation, only electrons pertaining to the totally symmetric representation contribute to $\rho(0)$. The quadrupole splitting ΔEQ for ^{57}Fe in axial symmetry is given by [16]:

$$\Delta EQ = 1/2e^2qQ \tag{8}$$

where Q is the quadrupole moment of the nucleus with spin I=3/2 in the excited state of the 14.4 keV Mössbauer transition and q is the electric field gradient [17]:

$$q = -\int \rho(\vec{r})(3z^2 - r^2)/r^5 d\vec{r} + \sum_q Z_q(3z_q^2 - r_q^2)/r_q^5 \tag{9}$$

The first term is the electronic contribution, calculated in the DVM method as a sum over the 3-dimensional grid, and the second term is the point-charge contribution of the neighbor N and H nuclei.

The contributions to the magnetic hyperfine field [18] are the Contact or Fermi H_c, given by:

$$H_c = 8\pi/3 g_e \mu_B [\rho_\uparrow(0) - \rho_\downarrow(0)] \times 1/2 \tag{10}$$

where g_e is the electronic spectroscopic factor, μ_B the Bohr magneton and the term in brackets is obtained with Eq. 2. The dipolar field H_D is defined as [19]:

$$H_D = g_e \mu_B \int [\rho_\uparrow(\vec{r}) - \rho_\downarrow(\vec{r})](3z^2 - r^2)/r^5 d\vec{r} \times 1/2 \tag{11}$$

where the densities are given by Eq. 2 and the integral is a sum over the 3-dimensional grid. Finally, the orbital contribution H_L is defined as:

$$H_L = g_e \mu_B \int \rho(\vec{r})(\vec{\ell}/r^3) d\vec{r} \tag{12}$$

so that the total measured hyperfine field H_F is:

$$H_F = H_c + H_D + H_L.$$

In Table IV are shown the results obtained for the Mössbauer parameters described above. To derive δ, we first performed calculations for free Fe atoms and ions, for which δ was measured in frozen gas matrices [20], also with a Density Functional self-consistent method. The results are plotted in Fig. 3 (only 3s and 4s contributions are considered, since $\rho(0)$ for the inner electrons do not show significant changes for different configurations and thus cancel out). The negative slope is due to the negative sign of $\Delta\langle r^2\rangle$ for the 14.4 keV transition of ^{57}Fe (see Eq. 7). From this plot, the value $\alpha = -0.228$ mm/s.a_o^{-3} is obtained, well within the range of "acceptable" values for Fe [21, 22]. Employing the equation derived for the line in Fig. 3 ($\delta = -0.228\rho(0) + 33.638$), the numbers for δ given in Table IV were obtained, using the molecular values of $\rho(0)$.

For all configurations, δ is much higher than would be obtained for Fe $3d^64s^2$, as may be seen from Fig. 3. The values are clustered slightly above the one for Fe^{+1} $3d^64s^1$. This is coherent with the Fe configurations in Table I ($\sim 3d^{6.6-7.0}4s^1$): the smaller charge on

Fe, due to larger 3d population, decreases $\rho(0)$ (increases δ) due to shielding of the 3s and 4s electrons by the 3d.

The values of ΔEQ are also shown in Table IV. Since the sign of the experimental value was also determined [2], this constitutes a valuable test for the ^{5}E ground state found. In fact, electrons in 3d orbitals pertaining to different spherical harmonics differ largely in both sign and magnitude of the electric field gradient q [16]. This may be verified in the large spread of calculated ΔEQ values for the different configurations, which differ among themselves in the occupation of 3d orbitals.

The value of Q utilized to calculate ΔEQ was 0.20b [16]. Although there is always a degree of uncertaining in any chosen value, one may expect this not to be far from the exact one. It may be thus seen that the ^{5}E ground state configuration **2** is indeed the one that gives the calculated ΔEQ closest to experiment. Configuration **2**, as discussed previously, is a mixture of **3** and **3'**, for which ΔEQ has the right sign but is too small and too large in magnitude, respectively. All other configurations give ΔEQ very far from the experimental value.

As for the magnetic hyperfine field, unfortunatly it was not possible to determine the sign experimentally, the two possible values being +800 or -900 kOe [2]. The values calculated and displayed in Table IV are the sum of the Contact field H_c and the dipolar field H_D. They are all very large and with positive or negative signs. Positive fields H_c correspond to configurations where the $10a_1\uparrow$ (4s) orbital is occupied; since the counterpart $10a_1\downarrow$ is not occupied, the positive field generated is very large (see Eq. 10). The core field H_c of Fe (1s, 2s and 3s) is negative [23], but not large enough to counterbalance the positive contribution of $10a_1\uparrow$. The large negative values of H_c for configurations **4** and **5** stem from the negative magnetic moments on the 4s orbital (larger $4s\downarrow$ population) which results in negative valence contributions to H_c, added to the negative core fields. The orbital field H_L (Eq. 12) could not be obtained with the present calculations, since it requires the inclusion of the spin-orbit interaction. Without this term, the direction of $\vec{\ell}$ relative to the spin remains undetermined. We calculated the maximum magnitude of H_L, utilizing Eq. (12), for the ^{5}E ground state; this corresponds to $\vec{\ell}$ and $\vec{s}$ being aligned. The number found was $\pm$436kOe; if the posivitive value is added to +568 kOe ($H_c + H_D$), the result would not be far from the experimental +800kOe. For configurations **5** and **6**, $H_L = 0$ due to the non-degenerate ground state [18].

It must be kept in mind, when comparing theoretical values with experiment, that the calculations did not take into account the effect of the environment of solid ammonia upon the measured Mössbauer hyperfine interactions.

5 Conclusions

The theoretical investigation of $FeNH_3$, performed with the Density Functional Discrete Variational Method, demonstrated that the ground state is a ^{5}E. The pertaining configuration presents a small mixture of Fe 3d(xz,yz) with 3d(xy,x^2-y^2); this proves to be essential in understanding the value of the measured quadrupole splitting. The configuration on Fe for the ground state is $\sim 3d^{6.6}4s^{1.1}$. The value for the isomer shift found is not far from the experimental value, and confirms the Fe configuration obtained. The

calculated quadrupole splitting compares well with experiment. The contact magnetic hyperfine field for the ground state is large and positive, due to the unbalanced occupation of a spin-up molecular orbital of predominantly 4s character.

Figure Captions

Figure 1 – Total energies of several configurations of $FeNH_3$ as a function of the Fe-N interatomic distance. Energies were shifted by an arbitrary value. Numbering of configurations as in Table I.

Figure 2 – Energies of the valence molecular orbitals of $FeNH_3$ as a function of the Fe-N interatomic distance, for the ^5E ground state (configuration **2**). Orbitals were labelled according to the major 3d or 4s contribution. Fe-N distance=1.98$\mathring{A}$.

Figure 3 – Isomer shifts versus electron density at the nucleus (3s and 4s) for Fe atom and ions. Values of δ from Ref. 20, relative to Fe metal.

Table Captions

Table I – Configurations, states, charges, magnetic moments and populations for $FeNH_3$, for calculations at the equilibrium distances.

Table II – σ, π and δ 3d populations for configurations of $FeNH_3$. Configurations numbered as in Table I; calculations at the equilibrium distances.

Table III – Population analysis for the valence orbitals of the ^5E ground state (configuration **2**) of $FeNH_3$. Fe-N interatomic distance=1.98$\mathring{A}$.
a) Only populations > 5% were included. Orbitals adding > 100% include small negative H 2p populations, due to strongly antibonding nature.

Table IV – Calculated and experimental Mössbauer hyperfine parameters of $FeNH_3$, for calculations at the equilibrium distances.
a) From Ref. 2; δ relative to Fe metal at room temperature;
b) From Ref. 24; δ relative to Fe metal;
c) Theoretical values of $H_F = H_C + H_D$.

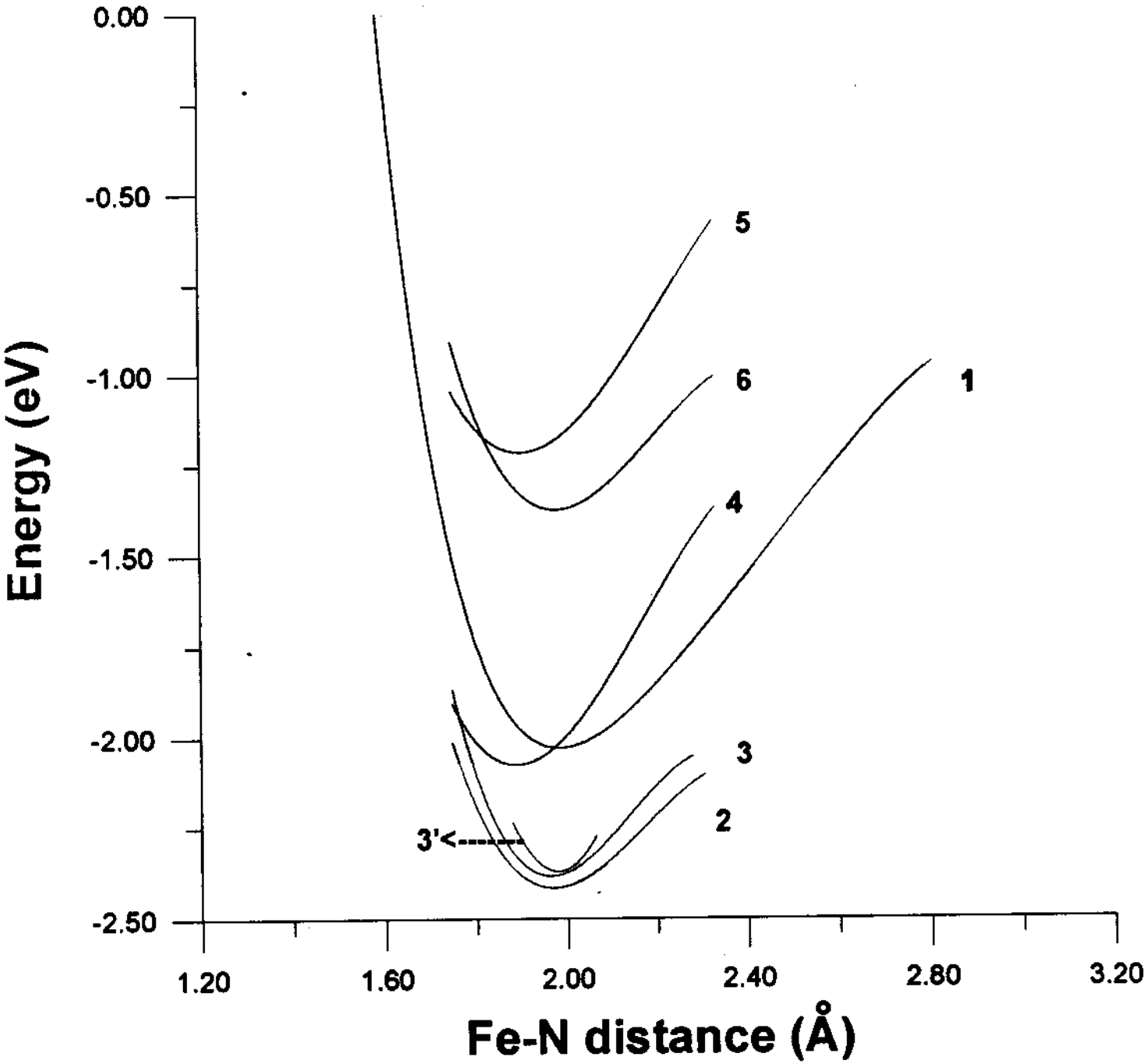
0.00
-0.50
-1.00
-1.50
-2.00
-2.50
Energy (eV)
1.20
1.60
2.00
2.40
2.80
3.20
Fe-N distance (Å)
1
2
3
3'
4
5
6

Fig. 1

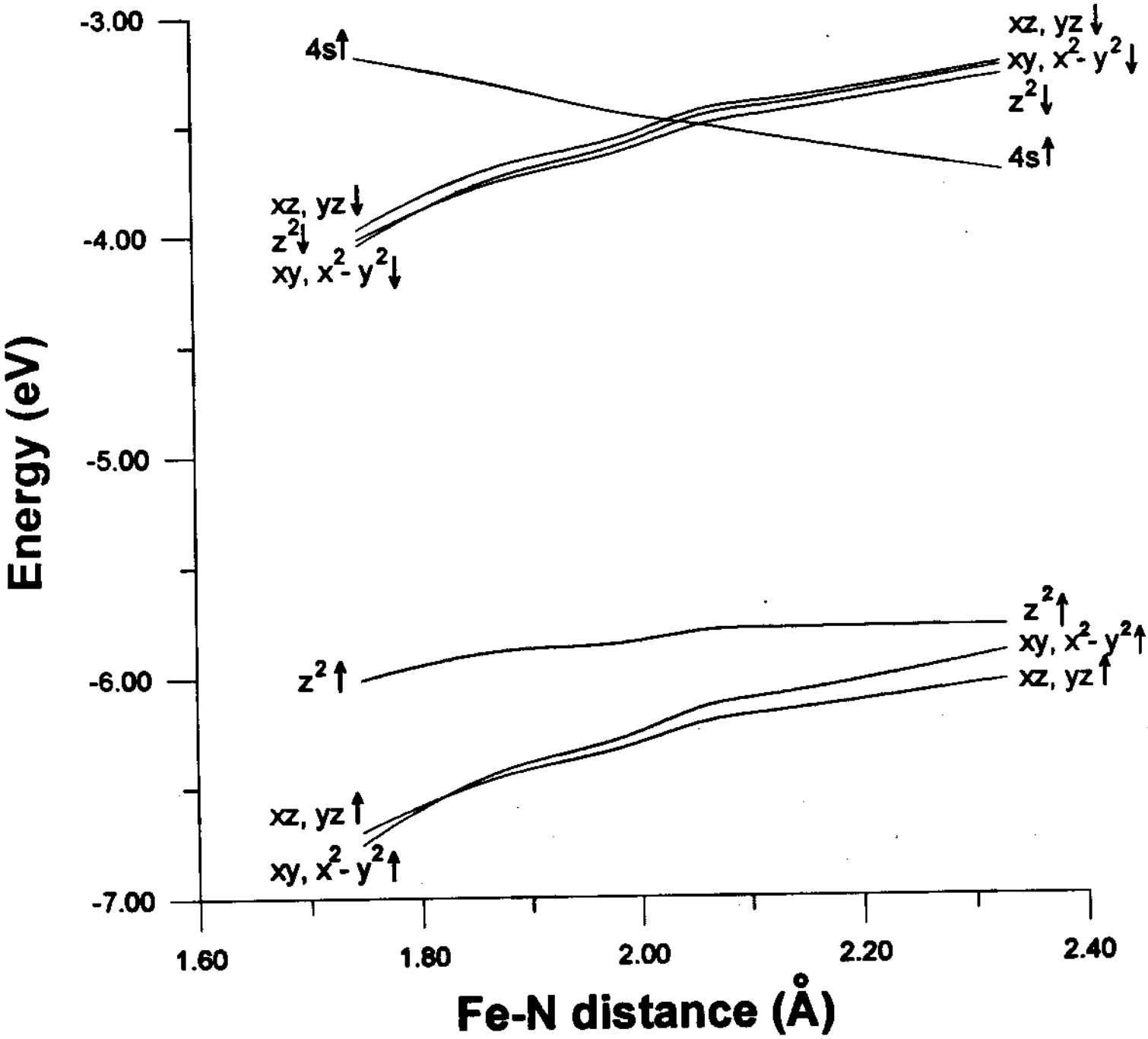
-3.00
-4.00
-5.00
-6.00
-7.00
Energy (eV)
4s↑
xz, yz↓
z²↓
xy, x²- y²↓
xz, yz↓
xy, x²- y²↓
z²↓
4s↑
z²↑
z²↑
xy, x²- y²↑
xz, yz↑
xz, yz↑
xy, x²- y²↑
1.60
1.80
2.00
2.20
2.40
Fe-N distance (Å)

Fig. 2

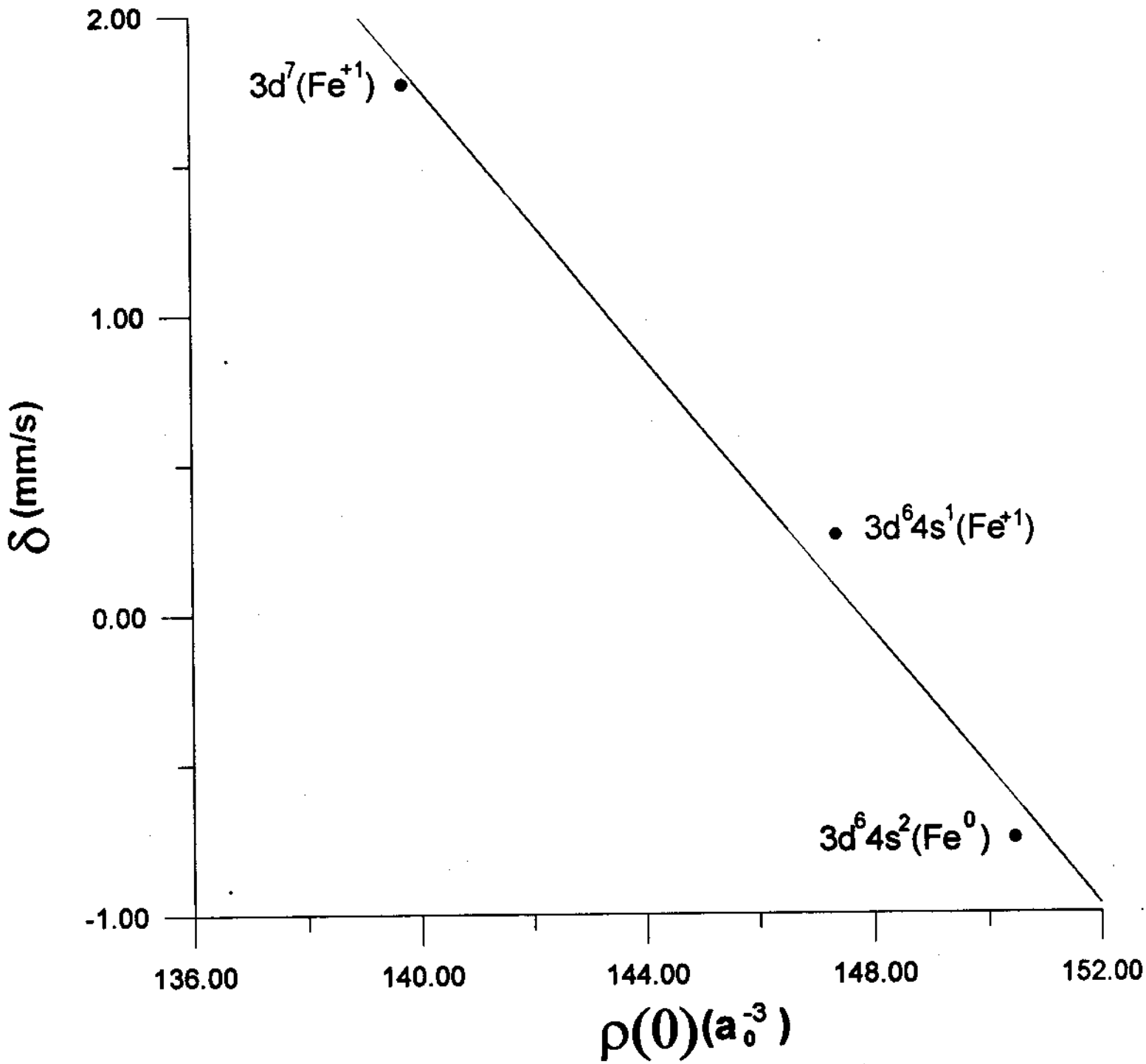
2.00
1.00
0.00
-1.00
δ (mm/s)
3d7(Fe+1)
3d64s1(Fe+1)
3d64s2(Fe0)
136.00
140.00
144.00
148.00
152.00
ρ(0)(a0-3)

Fig. 3

Table I

Configuration	States	Charge		Magnetic Moment (μ_B)		Fe populations		Fe orbital moments (μ_B)
		Fe	N	Fe	N			
(1) (↑) $9a_1^1 10a_1^1 4e^2 5e^2$ (↓)$4e^1\ 5e^1$	$^5A_1+^5A_2+^5E$	+0.16	-1.97	3.76	0.15	3d	6.94	2.92
						4s	0.84	0.79
						4p	0.07	0.06
(2) (↑)$9a_1^1 10a_1^1 4e^2 5e^2$ (↓)$9a_1^1 4e^1(xy,x^2\text{-}y^2)$	^5E	+0.22	-1.98	3.77	0.20	3d	6.63	3.28
						4s	1.12	0.47
						4p	0.04	0.04
(3) (↑)$9a_1^1 10a_1^1 4e^2 5e^2$ (↓)$9a_1^1 5e^1(xy,x^2\text{-}y^2)$	^5E	+0.22	-1.98	3.78	0.20	3d	6.64	3.28
						4s	1.11	0.47
						4p	0.05	0.04
(3') (↑)$9a_1^1 10a_1^1 4e^2 5e^2$ (↓)$9a_1^1 5e^1(yz,xz)$	^5E	+0.22	-1.97	3.74	0.23	3d	6.58	3.32
						4s	1.18	0.40
						4p	0.04	0.03
(4) (↑)$9a_1^1 4e^2 5e^2$ (↓)$9a_1^1 4e^1 5e^1$	$^3A_1+^3A_2+^3E$	+0.03	-1.81	1.99	-0.05	3d	6.93	2.49
						4s	1.03	-0.48
						4p	0.02	-0.02
(5) (↑)$9a_1^1 4e^2 5e^2$ (↓)$9a_1^1 5e^2(xy,x^2\text{-}y^2)$	$^3A_2$	+0.12	-1.90	1.95	-0.07	3d	7.02	2.63
						4s	0.85	-0.66
						4p	0.02	-0.01
(6) (↑)$9a_1^1 10a_1^1 4e^2 5e^2$ (↓)$5e^2(xy,x^2\text{-}y^2)$	$^5A_2$	+0.17	-2.00	3.76	0.13	3d	6.95	2.94
						4s	0.83	0.78
						4p	0.07	0.06

Table II

Configuration	3d population		
	$d_\sigma(z^2)$	d_π(xz,yz)	d_δ(xy,x^2-y^2)
1	1.00	2.95	2.98
2	1.66	2.17	2.81
3	1.66	2.01	2.97
3'	1.62	2.99	1.99
4	1.02	2.95	2.96
5	1.14	2.00	3.88
6	1.02	1.99	3.92

Table III

Orbital	Energy (eV)	Occupation	Population analysis[a] (in % of one electron)
$8a_1 \uparrow$	-10.72	1	13 Fe d(z^2), 5.5 N 2s, 87.9 N 2p(z)
$8a_1 \downarrow$	-10.22	1	6.6 Fe d(z^2), 6.6 N 2s, 94.6 N 2p(z)
$4e \uparrow$	-6.32	2	97.9 Fe d(xz,yz)
$5e \uparrow$	-6.28	2	98.6 Fe d(xy,x^2-y^2)
$9a_1 \uparrow$	-5.85	1	79.1 Fe d(z^2), 8.4 N 2p(z), 5.2 Fe 4s
$9a_1 \downarrow$	-3.62	1	28.7 Fe 4s, 62.4 Fe d(z^2)
$4e \downarrow$	-3.59	1	17.4 Fe d(xz,yz), 81.9 Fe d(xy,x^2-y^2)
$10a_1 \uparrow$	-3.44	1	91.9 Fe 4s, 5.9 Fe 4p(z), 5.9 Fe d(z^2)

Table IV

Configuration	δ (mm/s)	ΔEQ (mm/s)	H_c (kOe)	H_D (kOe)	$H_F^{(c)}$ (kOe)
1	+0.74	+0.16	+1224	+94	+1318
2	+0.42	-1.66	+539	+29	+568
3	+0.43	-0.59	+552	+66	+618
3'	+0.32	-7.27	+438	-167	+271
4	+0.50	+0.64	-810	-7	-817
5	+0.66	+6.40	-1088	+248	-840
6	+0.77	+6.81	+1193	+333	+1526
Experimental	+0.67[a]	-2.0[a]			+800 or -900[a]
	+0.60(5)[b]	|1.90(5)|[b]			

References

[1] K. Tamaru, Acc. Chem. Res. **1988**, 21, 88, and references therein.

[2] E.M. Baggio Saitovitch, J. Terra and F.J. Litterst, Phys. Rev. B **1989**, 39, 6403.

[3] R.G. Parr and W. Yang, "Density-Functional Theory of Atoms and Molecules", Oxford University Press, N. York (1989).

[4] D.E. Ellis and G.S. Painter, Phys. Rev. **1970**, B2, 2887; D.E. Ellis, Int. J. Quant. Chem. **1968**, S2, 35; E.J. Baerends, D.E. Ellis and P. Ros, Chem. Phys. **1973**, 2, 41.

[5] U. von Barth and L. Hedin, J. Phys. C **1972**, 5, 1629.

[6] B. Delley and D.E. Ellis, J. Chem. Phys. **1982**, 76, 1949.

[7] B. Delley, D.E. Ellis, A.J. Freeman, E.J. Baerends and D. Post, Phys. Rev. B **1983**, 27, 2132.

[8] C. Umrigar and D.E. Ellis, Phys. Rev. B **1980**, 21, 852.

[9] A.H. Stroud, "Approximate calculation of multiple integrals", Prentice-Hall, N. Jersey (1971).

[10] G. Herzberg, "Electronic Spectra of Polyatomic Molecules", Van Nostrand Reinhold, N. York (1966); cited in C.W. Bauschlicher, J. Chem. Phys. **1986**, 84, 260.

[11] J. Terra, unpublished.

[12] S.R. Langhoff, C.W. Bauschlicher, Jr., H. Partridge and M. Sodupe, J. Phys. Chem. **1991**, 95, 10677.

[13] C.E. Moore, "Atomic Energy Levels", US Natl. Bur. Stand. (US) 1952.

[14] T. Ziegler, Chem. Rev. **1991**, 91, 651.

[15] I. Pápai, J. Mink, R. Fournier and D.R. Salahub, J. Phys. Chem. **1993**, 97, 9986; and references therein.

[16] N.N. Greenwood and T.C. Gibb, "Mössbauer Spectroscopy", Chapman and Hall, London (1971).

[17] D. Guenzburger and D.E. Ellis, Phys. Rev. B **1980**, 22, 4203; D.E. Ellis, D. Guenzburger and H.B. Jansen, Phys. Rev. B **1983**, 28, 3697.

[18] A. Abragam, "The principles of nuclear magnetism", Oxford University Press, Oxford (1961).

[19] D. Guenzburger and E.M.B. Saitovitch, Phys. Rev. B **1981**, 24, 2368.

[20] T.K. McNab, H. Miklitz and P.H. Barrett, Phys. Rev. B **1971**, 4, 3787; P.A. Montano, P.H. Barrett and Z. Shanfield, J. Chem. Phys. **1976**, 64, 2896; H. Micklitz and P.H. Barrett, Phys. Rev. Letters **1972**, 28, 1547.

[21] "Mössbauer Isomer Shifts", ed. G.K. Shenoy and F.E. Wagner, North-Holland, Amsterdam (1978).

[22] D. Guenzburger and D.E. Ellis, Phys. Rev. B **1985**, 31, 93.

[23] D. Guenzburger, D.M.S. Esquivel and J. Danon, Phys. Rev. B **1978**, 18, 4561.

[24] P.H. Barrett and M. Pasternak, J. Chem. Phys. **1979**, 71, 3837.